

Advanced Kinetic-Based Modeling Applied to Plasma and Neutral Flows

Sergey Gimelshein, Natalia Gimelshein, and Jerry Brackbill

ERC, Inc., Edwards AFB, CA 93524

Jean-Luc Cambier and Andrew Ketsdever

Propulsion Directorate, Edwards AFB, CA 93524

Abstract

Chemical reactions between ions and electrons of a translated at high velocities field reversed plasmoid and neutral gas particles are examined in an adiabatic heat bath relaxation. Importance of different reaction mechanisms, such as charge exchange and electron impact ionization, is analyzed for conditions typical for FRC thrusters. These are gas and plasma densities on the order of 10^{18} molecule/m³, plasma temperatures between 5 and 50 eV, and relative velocities up to 30 km/s. Then, an implicit Particle-In-Cell code, Celeste3D, extended to include plasma-neutral and neutral-neutral elastic and inelastic processes and Coulomb collisions, is used to model a planar flow between an FRC plasmoid initially at a Schmid-Burgk equilibrium, and neutral gas with varying relative velocities, plasma temperatures, and neutral gas densities. The contribution of charge exchange and electron impact ionization reactions is analyzed, and the sensitivity of the entrainment efficiency to the plasmoid translation velocity and neutral density is evaluated.

1 Introduction

One of the most promising, and at the same time challenging, propulsion technologies is gh-power electric propulsion. The first challenge is associated with the necessity to operate a thruster at very high efficiency, otherwise the system limitations due to heat rejection become insurmountable. It is clear that high power can be efficiently delivered into a plasma by raising its temperature, i.e. its specific energy; consequently, the specific impulse can take large values, even in the excess of 10,000 sec. However, for a fixed power available, this also translates into small thrust and acceleration. While such a high I_{sp} may be highly desirable for deep space missions, the low-Earth orbit/Geosynchronous Earth orbit environments in which the US Air Force operates is mostly characterized by two competing requirements, i.e. (1) minimization of propellant and system mass (high I_{sp}) and (2) minimization of the time required for achieving the orbital maneuver (high thrust). Following the “goldilocks” principle, one must find the optimal range of I_{sp} which, depending on the mission, is usually between 2-5 ksec. The second challenge is therefore to design an electric propulsion (EP) system which can operate in that regime at high power (100-200 kWe). Finally, it would be beneficial to to operate in a dual mode, i.e. be able to tune the regime between higher thrust/lower I_{sp} and lower thrust/higher I_{sp} , at constant power and efficiency, thus presenting a third challenge.

Plasma at high temperature inevitably becomes highly ionized; this is very beneficial for coupling with external electro-magnetic fields and high-efficiency thrust generation. Typical losses associated with the plasma in these conditions include: (a) radiation; (b) “effective” ionization cost; (c) loss of confinement. The amount of energy lost to radiation depends strongly on the conditions, but generally speaking, the line transitions are self-absorbed while the plasma is closer to being optically thin for continuum radiation. The integrated bremsstrahlung emission is only weakly proportional to temperature and the radiative capture rate (free-bound transitions) decreases at high temperature; nevertheless, the rate of radiative

cooling can be problematic for high- Z plasma (due to a Z^2 dependence) and in radiative non-equilibrium conditions (volumetric emission).¹ The effective ionization accounts for the amount of energy required to produce an ion by electron impact, accounting for all other couplings which can reduce the electron energy; these include elastic collisions as well as all electronic excitations, and vibrational excitations in the case of molecular plasma. From dependence with respect to electron energy of the cross-sections for these various processes, the most efficient regime is obtained for electron temperatures of the order of 50 eV. Finally, particle confinement strongly depends on applied magnetic fields, since the cross-field diffusion scales approximately² as $1/B$.

Therefore, the optimal conditions are achieved for low- Z plasma at high (50-100 eV) temperature and in strong magnetic fields. These conditions are typically obtained in Field Reversed Configuration (FRC) plasma. The FRC is a self-organized magnetized plasma structure in the shape of a highly compact toroid. The magnetic field is mostly in the poloidal direction, generated by internal (toroidal) currents. The ratio of plasma pressure to magnetic pressure (β) is close to unity, i.e. the highest plasma density that can be attained for given external magnets. The poloidal field also contributes to the particle confinement. Starting from a background uniform plasma at a constant axial (bias) field, the FRC can be formed by pulsing external coils and reversing the applied field, inducing currents at the plasma boundary and “pinching” the plasma at both ends (see Fig. 1, left). The initial bias field is trapped inside the plasma and forced to reconnect at the end points (separatrix), creating an elongated toroidal shape (see Fig. 1, right).

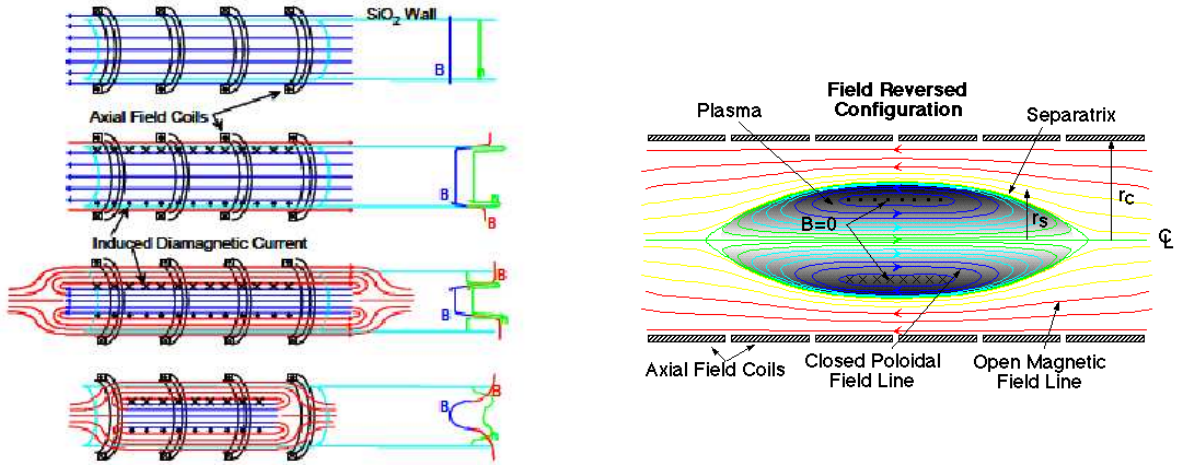


Figure 1: Schematics of basic FRC formation by field reversal (left) and schematics of an FRC plasmoid after formation, where the crosses indicate the toroidal plasma current (right).

In contrast to some other high- I_{sp} plasma propulsion concepts,³ the FRC is completely magnetically insulated from the external field; in other words, the plasma is not tied to an external field line, and the FRC can readily detach from the confining external field. It can also be translated and accelerated by applying a gradient of magnetic pressure using pulsed external coils. The FRC can therefore be efficiently accelerated to provide thrust, operates at a temperature that is optimal for ionization and is well confined. The basic concept of operations has been demonstrated⁴ and more recent research has led to further optimization of the formation process,⁵ while methods for increased efficiency through energy recovery in the electrical circuits are currently being developed under an AFOSR-STTR program.

One of the latest design iterations⁶ provides plasma velocities in the 10-40 km/sec range, a desirable regime for USAF applications. However, power and mass utilization efficiencies still remain to be determined more precisely and thrust augmentation is still desired. Since the plasma density in the FRC is close to optimal ($\beta \approx 1$), this could be achieved in two ways: (a) increasing the molecular mass of the propellant; (b) increasing the “effective” mass by gas entrainment. The first approach is by far the

easiest to achieve and one would presume that the common propellant of choice for EP (xenon), having the largest mass of any (stable) noble gas would be an ideal candidate. However, as previously mentioned, a high- Z plasma has higher rates of radiative and collisional (effective ionization cost) energy losses, thus reducing the efficiency. The second approach is tentatively more attractive but more difficult to achieve. In this case, the FRC propagates into an ambient gas and captures or pushes this neutral gas while being accelerated by the external coils. In this fashion, the system is able to exert a force on a composite object with a higher mass, while the plasma itself is kept at optimal physical conditions for high efficiency. The dynamics of the entrainment, momentum coupling and mixing processes at the FRC/gas interface are critical to the efficiency of this concept. It should be emphasized here that this process is also key to determining the true mass utilization efficiency of the FRC thruster by itself: there is always some level of residual, ambient neutral gas in the chamber as a consequence of gas injection, whether from the previous pulse or the current one. By deliberately introducing more gas to be acted upon by the FRC formed at the end of the injection cycle, one can thus potentially improve the thrust density while remaining at peak efficiency.

In this work, the process of neutral entrainment of an FRC plasmoid is studied numerically, with the main focus on the analysis of the relative importance of the electron impact ionization and charge exchange reactions between the neutral and charged particles. First, the balance between ionization and charge exchange reaction rates is examined for various gases and temperatures. Then, a study of heat bath relaxation is performed and the impact of Coulomb collisions is clarified. Finally, a Celeste3D particle-in-cell computational tool,⁷ extended to include the interactions between the charged and neutral particles and neutral particle transport, as well as Coulomb interactions between charged particles, is used in simulations of an FRC plasmoid and neutral gas interaction.

2 Rates of reactions involving charged particles

According to Ref. 4,8, the plasmoid temperature is expected to be less than 20 eV, and in some cases may cool to as low as 5 eV. Let us examine the rates of the different processes occurring in plasma at the temperature range of interest. The following processes are considered:

1. Electron impact ionization (EII, $A + E \rightarrow A^+ + e + e$). The electron impact ionization rates k_{eii} are obtained by the integration of the translational energy-dependent cross sections σ_{eii} tabulated in SIGLO database⁹ as

$$k_{eii} = \int g \sigma_{eii}(g) f_e(g) dg, \quad (1)$$

where g is the relative collision velocity and f_e is the Maxwellian distribution function.

2. Single charge exchange (SCX, $A^+ + A \rightarrow A + A^+$) For charge exchange reaction cross section, an expression from¹⁰ is used, written in CGS units as

$$\sigma_{scx} = \begin{cases} 0.5\pi a_0^2 \frac{Ry}{E_i} \log^2(100\sqrt{\frac{E_i}{\epsilon} \frac{\mu}{m_e}}) & \epsilon \geq \epsilon^* \\ \pi\sqrt{\alpha\epsilon^2/2\epsilon} & \epsilon < \epsilon^* \end{cases} \quad (2)$$

integrated to obtain the reaction rate similar to Eq. 1. Here,

$$\epsilon^* = \frac{2\alpha e^2}{a_0^4} \frac{E_i^2}{Ry^2} \left(\log \left(100\sqrt{\frac{E_i}{\epsilon^*} \frac{\mu}{m_e}} \right) \right)^{-4} \quad (3)$$

is a transcendental equation for ϵ^* , a_0 is the Bohr radius, E_i is the ionization energy, m and μ are particle mass and reduced mass, respectively, and α is the polarizability.

3. Recombination, including the radiative recombination in three-body collisions ($A^+ + e + e \rightarrow A + e$) and the radiative photorecombination ($A^+ + e \rightarrow A + h\nu$). The expressions from Ref. 11 are used,

which are, for the photorecombination, $k_{r1} = 2.7 \times 10^{-19} T_e^{-0.75}$ (m^3/s), and for the three-body recombination $k_{r2} = 8.75 \times 10^{-39} T_e^{-4.5} n_e$ (m^3/s). For the recombination reactions, an ion and electron number density of 10^{18} m^{-3} is assumed, similar to that observed in experiments of Ref. 4.

Charge exchange reactions are beneficial for neutral entrainment, because they produce a fast neutral particle that contributes to thrust, and a slow charged particle that can be quickly and efficiently accelerated by the electric field. On the contrary, the electron impact ionization, being highly endothermic reaction, takes away energy from the system and therefore lowers efficiency of the thruster.

The calculated reaction rates of these processes as function of temperature for light gas, helium are shown in Fig. 2 (left). It can be concluded that at those temperatures and a number density on the order of 10^{18} m^{-3} , the recombination is not important. The ionization reaction rate is lower than the charge exchange rate, which may be an indication that the entrainment process in a helium-based FRC thruster may be expected to be fairly efficient, especially for lower plasma temperatures. Note however that for temperatures below 10 eV and a typical plasmoid-neutral interaction time of $50 \mu\text{s}$, the fraction of ions that participate in a charge exchange reactions may be as low as 10% when the neutral density does not exceed 10^{18} m^{-3} . A higher neutral density will therefore be required to increase the number of charge exchange reactions and thus improve the efficiency of the neutral entrainment process. It can be seen that the ratio of EII rate and SCX rate for helium is favorable for neutral entrainment, however, the thrust of a helium-based thruster is relatively low, and using heavier species may be attractive.

One of potential candidates could be nitrogen, especially keeping in mind its air-breathing potential. The charge exchange, ionization, and recombination rates for nitrogen are shown in Fig. 2 (right). Note that for recombination rate, the dissociative recombination process ($\text{A}_2^- + e \rightarrow \text{A} + \text{A}^*$) is also included, that is the fastest mechanism of bulk recombination for molecules, with a rate of $k_{r3} = 1.0 \times 10^{-13} T_e^{-0.5} \text{ m}^3/\text{s}$. It can be seen that the plasmoid translation and entrainment is expected to be dominated by recombination at temperatures below $\sim 5 \text{ eV}$ and by the electron impact ionization at higher temperatures. The latter one is related to a relatively low ionization threshold of 15.6 eV as compared to the average energy in translational and internal modes of molecular nitrogen. The SCX rate for nitrogen is significantly lower than that of the other two processes over the whole temperature range of interest, so the use of nitrogen in FRC thruster may be problematic.

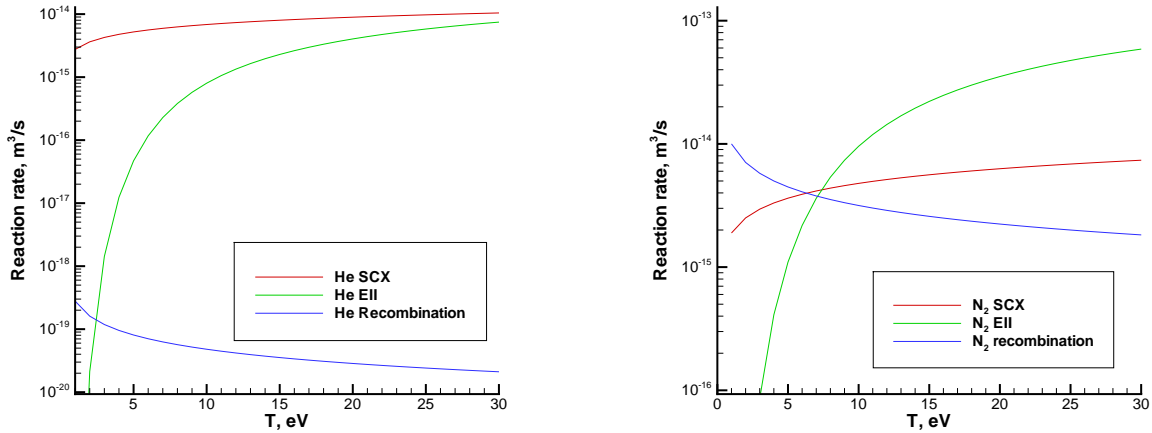


Figure 2: Plasma reaction rates in helium (left) and molecular nitrogen (right).

High thrust levels can be achieved using heavy particles, so xenon is often used in thrusters. However, because its ionization energy is low, the EII rate for xenon is about two orders of magnitude larger than that of SCX over the whole temperature range (see Fig. 2, left). Therefore, the efficiency of xenon-based FRC thruster is expected to be low.

Species with high ionization energy have low EII rate. One of such species is neon, whose ionization energy is equal to 21.6 eV. The charge exchange and ionization rates for neon are plotted in Fig. 3 (right). The recombination rate is not shown as it was found, similar to helium, to be much lower than the other two rates. The results show that the charge exchange reaction is expected to occur more often than the ionization, and for plasmoid temperatures on the order of 10 eV or lower the entrainment efficiency may be sufficiently high. Therefore, neon will be used in all subsequent calculations.

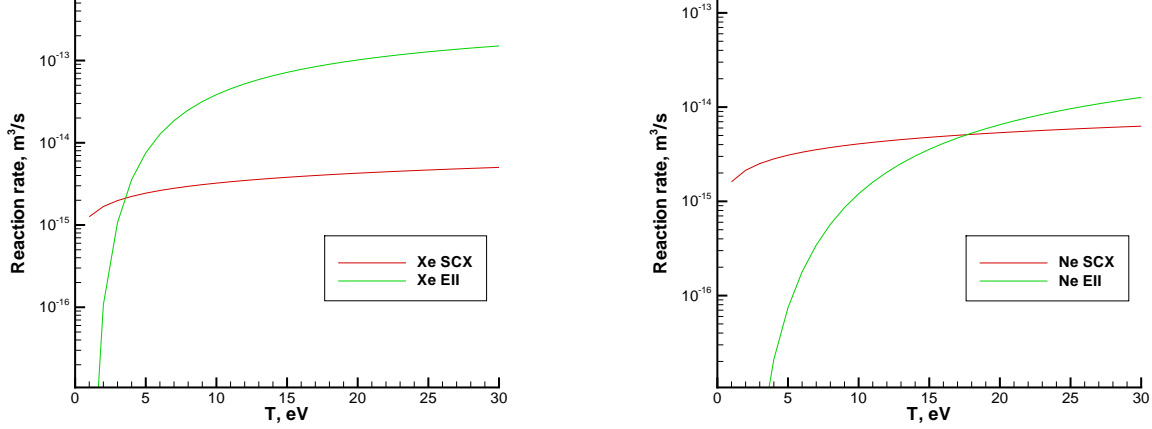


Figure 3: Plasma reaction rates in xenon (left) and neon (right).

3 Adiabatic relaxation of neon plasma

When cold stagnant neutral atoms collide with the fast moving plasma ions and electrons, the relaxation process that ensues depends on many factors such as plasma temperature, concentration of reacting species and the relationship between different reaction rates. Let us consider the effect of these factors on the time evolution of plasma and neutral properties in an adiabatic heat bath. Although the spatially homogeneous heat bath can not accurately predict the multi-dimensional evolution of plasma affected by the neutral flow, it nevertheless captures the main features of the relaxation process, and thus helps to understand the relative importance of various factors at play. To better model the neutral entrainment process, it is assumed that initially the neutral species and the charged species have relative velocity U . The dependence of the relaxation process characteristics on the magnitude of U is illustrated in Fig. 4. Unless otherwise noted, the initial plasma temperature is set to 10 eV, the neutral temperature is 300 K, and both neutral and plasma density are 10^{18} m^{-3} . The calculations are performed for the two different values of U , 20 km/s and 30 km/s.

Consider first the case of 20 km/s. In the absence of relative collision velocity, the ions and neutrals are expected to quickly relax to $0.5 * (T_{neut} + T_{ion}) \approx 5.01 \text{ eV}$. However, as the kinetic energy of relative motion of charged and neutral particles is converted into thermal energy, the temperature of all species increases, and heavy particles achieve thermal equilibrium at the temperature of about 12 eV (see Fig. 4, left). The thermal relaxation of electrons due to elastic collisions with neutrals and Coulomb collisions with ions is fairly slow, and the change in electron temperature is primarily related to the electron impact ionization reactions, which, being strongly endothermic, significantly decreases electron temperature.

For a higher relative velocity between charged and neutral species (30 km/s), due to higher values of the kinetic energy of relative motion, the final temperature of heavy species is over 20 eV. The electron temperature changes very little compared to the 20 km/s case. This is again related to the slow thermal relaxation of electrons, and small change in ionization rate as the relative electron/neutral velocity is

small compared to the thermal velocities of electrons, and the latter is the main contributor to ionization. The impact of relative velocity on electron temperature becomes visible only after $100 \mu\text{s}$. The important conclusion that can be drawn from these results is that for any flow velocity (and also for any plasma temperature) there is a strong thermal non-equilibrium between neutrals, electrons, and ions. Such a non-equilibrium is expected to occur in the actual neutral entrainment of an FRC thruster, and therefore a kinetic approach is best suited to model such an entrainment.

The number density of ions very weakly depends on the flow speed, (see Fig. 4, right) because number of ions changes only due to EII reactions, and, as stated earlier, their rates are not much affected by the flow speed. The initial electron temperature, however, is extremely important, as shown in Fig. 4 (right) for $U = 20 \text{ km/s}$. The electron temperature impacts the ionization rate, and when the initial plasma temperature is 5 eV , less than 3% of the neutral gas is ionized in about $30 \mu\text{s}$. To study the dependence of the relaxation process on the initial density of the neutrals, the calculation was performed with the initial number density of the neutrals equal to $3 \times 10^{18} \text{ m}^{-3}$. The number of charge exchange reactions for a plasma temperature of 10 eV and $U = 20 \text{ km/s}$ was found to linearly increase with neutral density. The dependence of the number of ionization reactions on neutral density is weaker than linear, as can be seen in Fig. 4 (right). When neutral density increases by a factor three, the ion density increase, primarily affected by the ionization process, is roughly a factor of three only in the first few microseconds. At $1000 \mu\text{s}$, the ion density change is only 25% higher than the baseline case. This is primarily related to the depletion of high energy electrons, as will be discussed below.

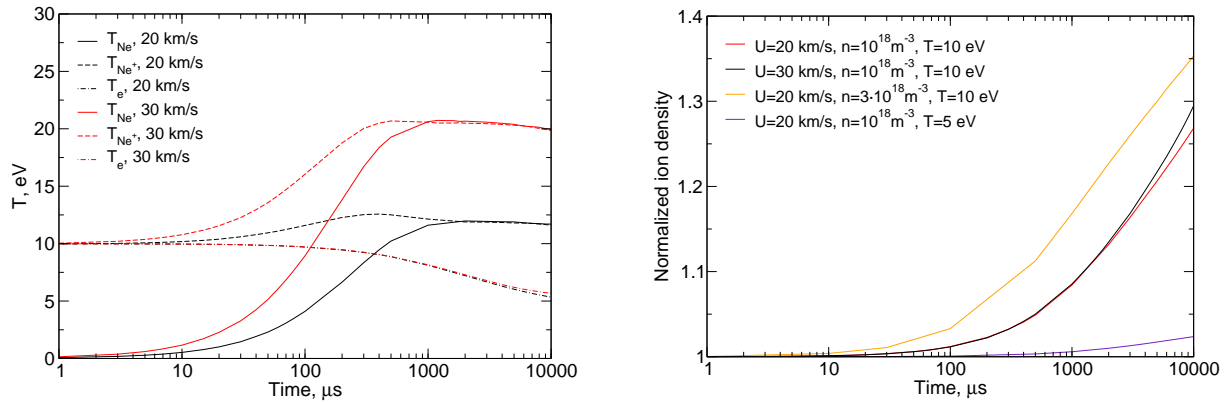


Figure 4: Impact of plasma parameters on the temperature of different species (left) and ion number density (right)

Generally, the electron impact ionization reactions results in energy transfer from the translational motion of reacting electrons and neutrals to the potential energy of newly formed electron and ion. The reaction therefore decreases plasma temperature, and in particular, depletes the high velocity tail of electrons. This, in turn, will slow down the electron impact ionization rate (but have only limited impact on charge exchange reactions). The main process that leads to the equilibration of the electron velocity distribution function is Coulomb collisions between electrons. When the Coulomb collisions are turned off, the high energy tail is quickly depleted by ionization, as illustrated in Fig. 5 (left). There is also noticeable impact of Coulomb collisions on the evolution of plasma density, shown in Fig. 5 (right) for $U = 20 \text{ km/s}$ and $T_{p,ini} = 10 \text{ eV}$. Note that such a non-equilibrium in velocity distribution is another indication that a kinetic approach is necessary to accurately model neutral entrainment in an FRC thruster. For a multi-dimensional neutral entrainment, when a translated plasmoid passes through neutral gas, the effects mentioned in this section, such as non-equilibrium, fast relaxation rates for high neutral density, strong influence of plasma temperature, the increase of ionization rate due to Coulomb collisions, etc, are expected to be even more pronounced, as the plasma particles collide with new, undisturbed neutral gas due to the plasmoid translation.

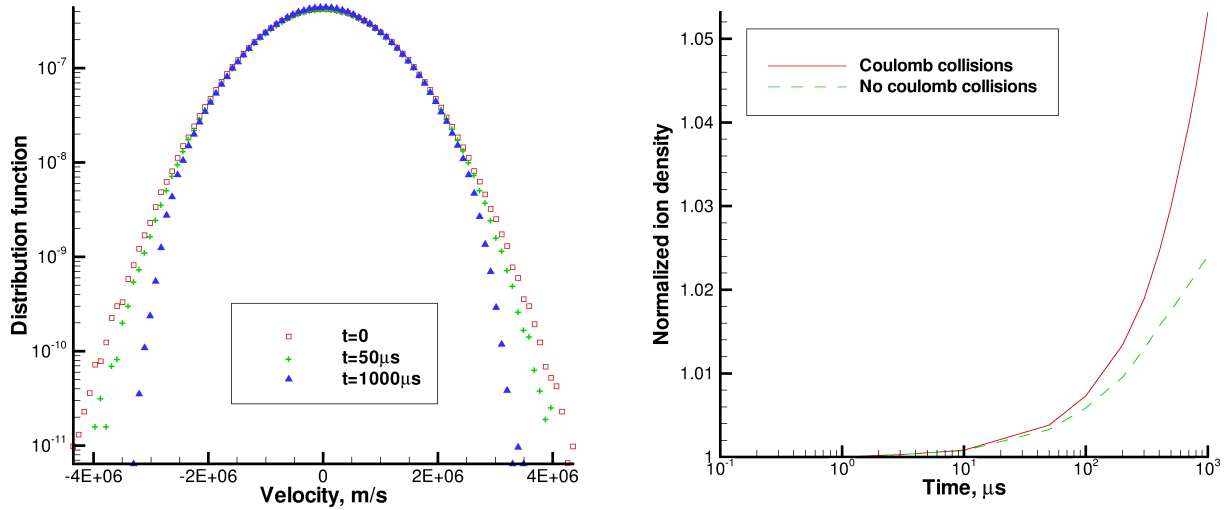


Figure 5: Depletion of electron velocity distribution function due to ionization when Coulomb collisions are turned off (left) and the effect of Coulomb collisions on plasma density evolution (right).

4 Numerical method and flow conditions for FRC entrainment

The computational tool that was used in this work to model the process of neutral entrainment of an FRC plasmoid is Celeste3D. Celeste3D is an implicit three-dimensional Particle-In-Cell (PIC) code that solves the full set of Maxwell-Vlasov equation and has been extensively used in the past for various astrophysical and laboratory plasma problems.^{12,13} The implicit moment formulation of the PIC method implemented in Celeste results in highly efficient simulations based on ion length and time scales, and not electron scales as explicit methods do, while retaining the kinetic effects of both the electrons and the ions. An explicit simulation requires the time step to be $\Delta t < 2/\omega_{pe}$, and the spatial cell size to be $\Delta x < \zeta\lambda_e$ in order to avoid the finite grid instability. Here, ω_{pe} is the electron plasma frequency, and λ_e is the electron Debye length. In an implicit simulation, these requirements are replaced by an accuracy condition related to the conservation of energy, $\Delta t < \frac{\Delta x}{c_e}$, where c_e is the electron thermal speed.

Original Celeste3D models the evolution of ion and electron populations as described by the Vlasov equation, coupled with the solution of full Maxwell equations; it does not simulate neutral particles. To study the neutral entrainment process, Celeste3D was extended to include neutral transport and collisional relaxation. A Direct Simulation Monte Carlo based capability has been added to Celeste that includes neutral transport and collisions. The following collision processes are included in this work: neutral-neutral collisions (modeled according to the VHS model¹⁵); the charge exchange reactions (the cross section is given earlier in this paper); neutral-ion elastic collisions (according to Ref.¹⁰ the cross section is twice the charge exchange cross section); the electron impact ionization (the cross section is also given earlier). The hard sphere after-collision scattering is assumed for all these processes, with the exception of charge exchange reactions, for which the velocities of neutrals and ions are swapped. As all species have different weights, a weighting scheme¹⁶ is applied. The majorant collision frequency¹⁷ of the DSMC method is used to model the collision process in cells. In addition to the neutral capability, a Coulomb collision module has been added to Celeste, based on a particle-weights scheme of Ref.¹⁸ (see previous section for more detail).

Although the actual entrainment geometry is three-dimensional, as a nearly axisymmetric plasmoid interacts with neutral gas supplied from two or more azimuthal injectors, three-dimensional PIC modeling is extremely time consuming, and in this work it was replaced by a 2D (planar flow). The result is a much larger number of particles per cell and thus smaller statistical scatter. The grid was 40×80 , and the number of simulated ions, electrons, and neutrals per cell was approximately 64, 100, and 512, respectively. Since the cost of an implicit simulation is a direct function of the electron mass (see

above, the computational time is inversely proportional to the square root of the electron mass m_e), the simulation efficiency may be further enhanced through the introduction of the weighted electron mass, $m'_e = Wm_e$, where the constant $W > 1$. The ion-to-electron mass ratio has to be high enough to preserve the kinetic effects, and the value of m_i/m'_e on the order of 100 is usually sufficient.¹² In this work, $m_i/m'_e = 100$ is used. The initial conditions used to set an equilibrium plasmoid is the a Schmid-Burgk equilibrium¹⁴ with the average plasma density of 10^{18} m^{-3} and two plasma temperature of 5 and 10 eV.

To simplify the inflow boundary conditions, the neutral-plasma interaction is examined in the reference frame of the plasmoid, so that the neutral gas is injected into the computational domain from the left boundary, and then passes through the domain from left to right. The properties of the injected neutral gas are changed to study their impact on the neutral-plasma interaction. In these computations, both periodic (10 eV plasmoid) and open (5 eV plasmoid) boundary conditions for plasma and open boundary conditions for neutrals were imposed at the left and right boundaries, and a conducting wall with specular reflection was set at the top and bottom boundaries. Note that computations were also performed with no neutral inflow to analyze the temporal evolution of the plasmoid; it was observed that the equilibrium is maintained for at least 10,000 ion plasma periods. This amounts to over $30 \mu\text{s}$ for the conditions under consideration, and is longer than the plasmoid-neutral interaction time.

5 Interaction of FRC plasmoid with neutral gas

The first set of computations is conducted for the average plasma density inside the plasmoid of $10^{18} \text{ molecule/m}^3$ and plasma temperature of 5 eV, with the neutral density of $10^{18} \text{ molecule/m}^3$ and a relative velocity U_{rel} of 20 km/s between the plasmoid and neutrals. As mentioned earlier, the plasmoid-neutrals interaction is modeled in the reference frame of the plasmoid, so that the plasmoid is initially not moving, and neutral gas is introduced into the computational domain with the bulk velocity of U_{rel} . Time evolution of neutral gas density is shown in Fig. 6 (left). The gas is injected from the left boundary, and the density is normalized by the free stream value. At the time moment of $8 \mu\text{s}$ after the beginning of the plasmoid/neutrals interaction, the neutrals advanced past the center of the computational domain into the region where the plasma density is maximum. Although there is some small decrease in neutral density due to electron impact ionization reactions as well as some backward scattering, this effect is fairly small at this point. However, at $12 \mu\text{s}$ it becomes more obvious, with the loss in neutral density reaching about 20% in the central part of the flow. As the neutrals reach the outflow boundary at time $16 \mu\text{s}$, this loss amounts to about 30%. Again, the loss is both due to elastic and inelastic interactions between neutral atoms and charged particles.

The field of ion density normalized by $10^{18} \text{ molecule/m}^3$ is shown in Fig. 6 (right) at the same time moments. Note that the electron density is nearly identical, except for some statistical scatter inherent in the approach. After the first $8 \mu\text{s}$, the impact of neutrals on the plasmoid is negligible as the ion density is almost symmetric with respect to $X = 0.15 \text{ m}$. At $12 \mu\text{s}$, the impact of neutrals on the plasmoid is manifested through a moderate, on the order of 5%, increase in plasma density in the region of maximum plasma density as a result of electron impact ionization, and a significant elongation of the plasmoid due to the momentum transfer between plasma and neutrals in charge exchange and elastic collisions. This effect is even more pronounced at $16 \mu\text{s}$, when the plasma density in the center decreases as the result of mass transfer in the direction of the neutral flow, Open boundary conditions at the left and right boundaries are used for these computations, and a significant loss of plasma particles though the outflow boundary is observed at $16 \mu\text{s}$,

Consider now the results of the interaction between a 10 eV plasmoid and neutral gas. Figure 7 (left) presents an instantaneous snapshot of ion density at a time of $15 \mu\text{s}$ after the neutral injection started for all cases except $U = 30 \text{ km/s}$, for which it is $10 \mu\text{s}$ after the start of injection (this is the time that the moving neutrals need to cross the computational domain). The ion number density presented in that figure is normalized by 10^{18} . For comparison, the result for a no-neutrals, plasma-only case is also shown (top quarter). Note that the no-neutral field practically does not change with time, with the exception of small changes related to the statistical scatter. The baseline case shown in the second quarter represents

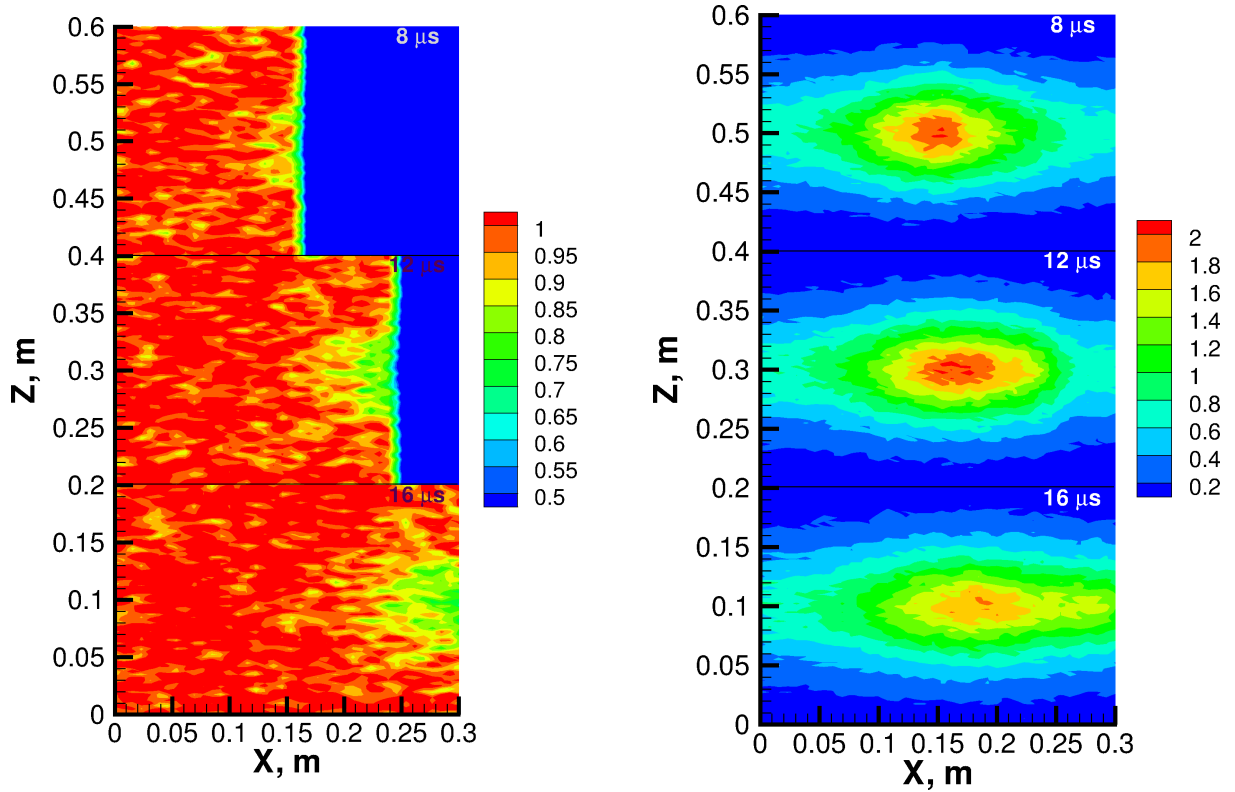


Figure 6: Neutral (left) and ion (right) density at different time moments.

the free stream neutral density of 10^{18} and velocity of 20 km/s, and the third and forth cases consider an increased neutral velocity and density, respectively. For the baseline case, the neutral-plasma interaction results in modest, slightly more than 5%, increase in the number of ions in the region where the ion density is near its maximum. This is obviously the result of electron impact ionization reactions. It is important to note that there is a clear translation of the plasmoid from the center of the computational domain to the right. The shift, which amounts to almost 2 cm, is due to the momentum transfer from the moving neutrals to the plasma particles. The average velocity of initially stationary plasmoid is about 3 km/s. Since the computations are conducted in the frame reference of the plasmoid, in application to the actual FRC entrainment configuration that means that the momentum is in fact transferred from the moving plasmoid to the neutral gas. For a higher relative velocity between the plasmoid and neutrals, $U = 30$ km/s, the plasma-neutral interaction is clearly weaker. The plasmoid is translated only at about 1 cm, and the number of neon ions is increased only by about 3%. The reason for this is a shorter interaction time due to a higher relative velocity between neutral and plasma particles. When the free stream neutral density is increased by a factor of three, the momentum transfer essentially triples, as does the number of ionization reactions. Note also that the shape of the plasmoid becomes more elongated for stronger neutral-plasma interaction.

The ion temperature increases for the baseline case by about 1.6 eV in most of the computational domain as compared to the plasma-only case, as illustrated in Fig. 7 right). Here and below, the temperature is in eV. The increase is much more pronounced, over 10 eV, for the $U = 30$ km/s case. This is related to the transfer of energy from the bulk neutral flow motion to the thermal motion of ions and neutrals, and is consistent with the conclusions of the Heat Bath section. Note that for $U = 30$ km/s the maximum ion temperature is observed to the right of the maximum ion density, where more ions have collided with electrons. For the elevated neutral density, there is a minimum ion temperature in this region, related primarily to the large number of endothermic ionization reactions (for the baseline case,

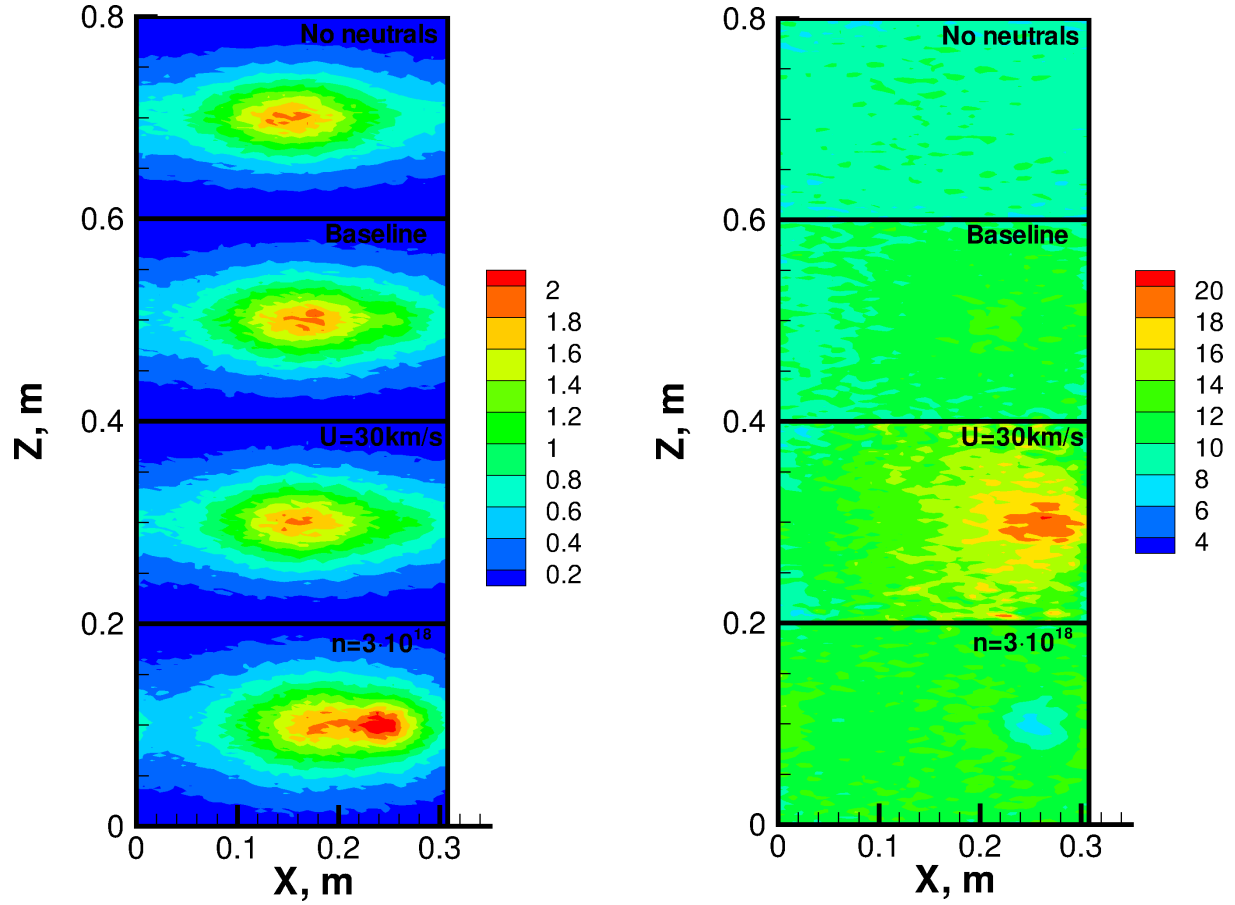


Figure 7: Ion density (left) and temperature (right) for different free stream conditions.

there is a temperature minimum in this region, too, although less pronounced). The number density of neutral particles, normalized by its free stream value, is plotted in Fig. 8 (left). It can be seen that the neutral flow, moving from left to right, almost reached the right boundary of the computational domain. Most importantly, the interaction of neutral particles with ions and electrons depleted their population in the central region by almost 50% for the baseline and elevated density cases, and by over 30% for $U = 30$ km/s. Recalling that the absolute change in ion density is much smaller than the change in neutral density, it becomes clear that the latter is related to charge exchange reactions. The neutral particles lose their momentum in X direction after charge exchange reactions, and thus do not reach the right boundary. The temperature field of neutral particles, shown in Fig. 8 (right), indicates the region where neutrals mostly travel after they are created as a result of charge exchange reactions. It is the region of elevated temperature (relative velocity between these neutrals and free stream neutrals is high) observed mostly to the left of the center of the plasmoid, and away from the top and bottom conducting walls. Therefore, in the actual entrainment the neutrals are expected to travel with the plasmoid. Obviously, this is exactly the effect that the entrainment is used for.

6 Conclusions

This work is a step toward accurate modeling of a high-power electric propulsion thruster based on a high-speed neutral entrainment of a field reversed configuration plasmoid. A number of chemical and physical processes are important in the interaction between the plasmoid and neutral gas, and two of

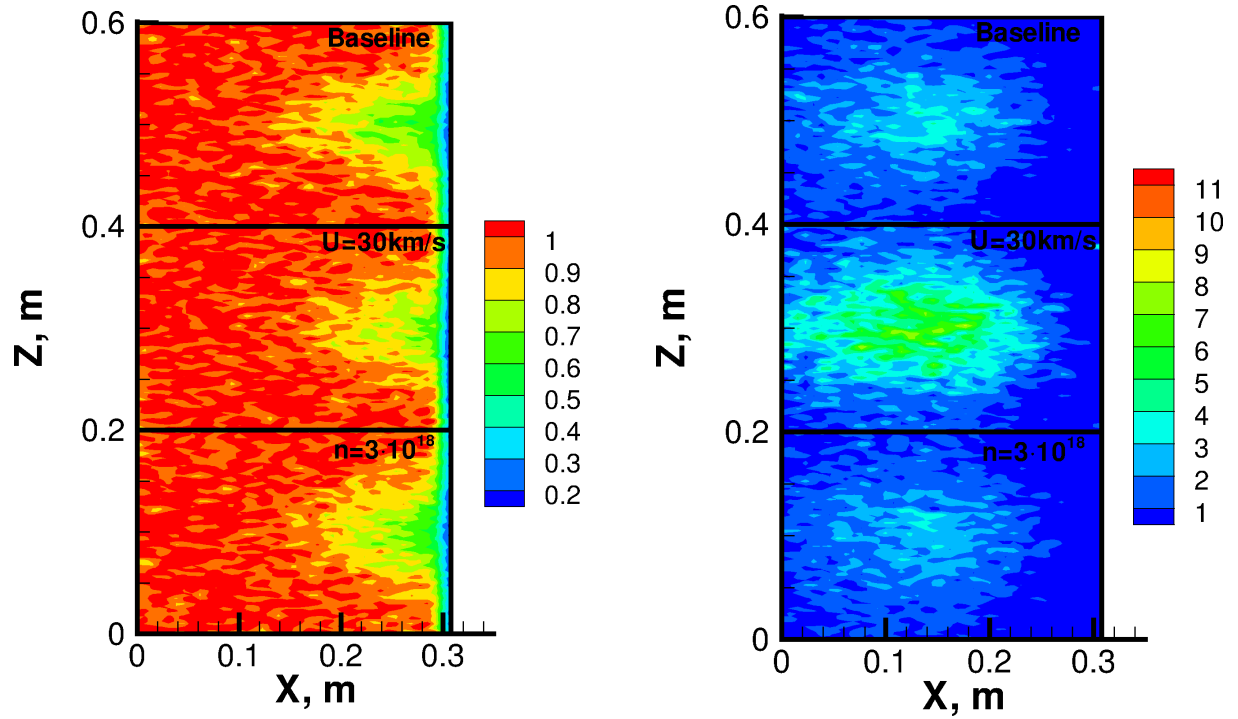


Figure 8: Neutral density (left) and temperature (right) for different free stream conditions.

them are considered here, charge exchange and electron impact ionization reactions. Both processes are expected to significantly affect the performance of an FRC thruster, with the former increasing thrust force and improving total thruster efficiency and the latter is likely decreasing them. Comparison of ionization and charge exchange reaction rates presented in this work indicates that the use of nitrogen and xenon may be problematic, while neon appears to be a fairly good propellant.

The computation effort presented in this work covered thermal relaxation in an adiabatic heat bath with neutral and plasma properties close to those of a typical FRC thruster, and a two-dimensional interaction of a 10^{18} molecule/m³, 5 to 10 eV FRC plasmoid, initially at a Schmid-Burgk equilibrium, and neutral gas with comparable density. The 0D computations showed that the relaxation process proceeds under conditions of strong thermal and chemical non-equilibrium; ion, electron, and neutral temperatures strongly differ, and the electron distribution function is non-Maxwellian. This indicates that a kinetic approach has to be used to model neutral entrainment in FRC thrusters. Strong impact of electron temperature on plasma density is shown in heat bath relaxation, mostly related to ionization reactions. Increase in relative velocity between plasma and neutrals strongly affects ion and neutral temperature. Electron impact ionization was found to deplete high velocity tail of the electron distribution function, and modeling of Coulomb collisions between electrons is desirable to properly account for that depletion.

Two-dimensional modeling of a an FRC plasmoid / neutral gas interaction is conducted with an implicit PIC code Celeste3D, extended in this work to include neutral transport, plasma-neutral and neutral-neutral collisions and Coulomb collisions. Neon propellant was used with a baseline plasma and neutral densities of 10^{18} m⁻³, plasma temperatures of 5 and 10 eV, and relative velocities of 20 and 30 km/s. For both plasma temperatures, the results show strong entrainment of neutral particles by a translated plasmoid as a result of charge exchange reactions between slow neutrals and fast moving ions, and a modest increase in plasma density due to electron impact ionization. The increase in neutral density appears highly beneficial in terms thruster efficiency as it proportionally increases the number of entrained neutrals. The increase in plasmoid velocity decreases that number due to a shorter plasma-neutral interaction time. Note that the present computations have not included the electronic excitation

and related processes, the effect of those is estimated to be similar to the electron impact ionization for plasmoid temperatures between 5 and 10 eV, and will be included in the future.

7 Acknowledgements

The work was supported by the Air Force Office of Scientific Research (Dr. Mitat Birkan).

References

- [1] McKenna K.F. et al., "Particle confinement scaling in field-reversed configurations", Phys. Rev. Lett. 50, 1787 (1983)
- [2] Rostoker N. and Qerushi A., "Classical transport in a field reversed configuration", Plasma Phys. Rep. 29(7), 626 (2003).
- [3] Elliott F., Foster J., and Patterson M., An Overview of the High Power Electric Propulsion (HiPEP) Project, AIAA Paper 2004-3453.
- [4] Kirtley D., Brown D., and Gallimore A. Details on an annular field reversed configuration plasma device for spacecraft propulsion, IEPC-2005-171.
- [5] Miller S., Rovey J. Progress in modeling of pre-ionization and geometric effects on a field-reversed configuration plasma thruster, AIAA 2009-3733.
- [6] Slough J., Kirtley D., and Weber T. Pulsed plasmoid propulsion: the ELF thruster, IEPC-2009-265.
- [7] Lapenta, J.U. Brackbill, Dynamic and Selective Control of the Number of Particles in Kinetic Plasma Simulations, Journal of Computational Physics, 115, 213-227, 1994.
- [8] Kirtley, D., Slough, J., Pihl, C., Meier, E., Milroy, R., Pulsed plasmoid propulsion: airbreathing electromagnetic propulsion, IEPC-2011-015.
- [9] I. C. Pitchford, J. P. Boeuf, and W. L. Morgan, User-friendly Boltzmann code for electrons in weakly ionized gas, in Proceedings of the IEEE International Conference on Plasma Science, Boston, MA, 1996 (IEEE, Piscataway, NJ, 1996).
- [10] S.A. Losev, S.O. Macheret, B.V. Potapkin, G.G. Chernyi, Physical and chemical processes and gas dynamics: cross sections and rate constants. Progress in Astronautics and Aeronautics, 196, AIAA, 2002.
- [11] Raizer Yu.P., Gas discharge physics, Springer-Verlag, Berlin Heidelberg, 1991
- [12] P. Ricci, G. Lapenta, J.U. Brackbill, GEM Challenge: Implicit Kinetic Simulations with the Physical Mass Ratio, Geophysical Research Letters, 29, 10.1029/2002GL015314, 2002.
- [13] Lapenta, G., Brackbill, J. and Ricci, P. Phys. Plasmas 13, 055904 (2006).
- [14] Schmid-Burgk, J. Finite Amplitude Density Variations in a Self-Gravitating Isothermal Gas Layer, Astrophysical Journal, vol. 149, 727-729 (1967).
- [15] Bird, G.A., *Molecular Gas Dynamics and the Direct Simulation of Gas Flows*. Clarendon Press, Oxford. 458 pp, 1994.
- [16] Gimelshein S.F., Levin D.A., Collins R.J. Modeling of Infrared Radiation in a Space Transportation System Environment. AIAA Journal, Vol. 40, No. 4, 2002, pp. 781-790.
- [17] Ivanov, M.S. and Rogasinsky, S.V., Analysis of the numerical techniques of the direct simulation Monte Carlo method in the rarefied gas dynamics, *Soviet J. Numer. Anal. Math. Modeling*, Vol. 3, No. 6, 1988, pp. 453-465.
- [18] K. Nanbu and S. Yonemura, Weighted Particles in Coulomb Collision Simulations Based on the Theory of a Cumulative Scattering Angle J. Comp. Phys, 145, 639-654 (1998)